CO adsorption on Ni(100) and Pt(111) studied by infrared–visible sum frequency generation spectroscopy: design and application of an SFG-compatible UHV–high-pressure reaction cell

G. Rupprechter *, T. Dellwig, H. Unterhalt and H.-J. Freund

Chemical Physics Department, Fritz-Haber-Institut der Max-Planck-Gesellschaft, Faradayweg 4-6, D-14195 Berlin, Germany
E-mail: rupprechter@fhi-berlin.mpg.de

Infrared–visible sum frequency generation (SFG) surface vibrational spectroscopy was applied to monitor CO stretching vibrations on Ni(100) and Pt(111) in the range from submonolayer coverages up to 200 mbar. Since SFG can operate in a pressure range from ultrahigh vacuum (UHV) to ambient conditions, it is particularly suited for *in situ* studies of adsorbates at elevated pressure or during a catalytic reaction. At high coverages, a compressed overlayer was formed on Ni(100) at 100 K that can be modeled by a coincidence structure. On Pt(111), terminally bonded (on-top) CO was the only species observed at 230 K, independent of gas pressure. At low pressure the SFG spectra were complemented by LEED, AES and TPD. The experiments were carried out in an SFG-compatible elevated pressure reactor that is attached to a UHV surface analysis chamber. After preparation and characterization in UHV, model catalysts can be transferred *in vacuo* into the reaction cell. The reactor is separated from the UHV chamber by an arrangement of differentially pumped spring-loaded teflon seals and can be pressurized to 1 bar without degrading the vacuum in the UHV analysis system.

KEY WORDS: carbon monoxide; adsorption; sum frequency generation; vibrational spectroscopy; high pressure cell; nickel; platinum; single crystals

1. Introduction

Catalysis science has greatly benefitted from the utilization of well-defined model catalysts and surface-sensitive techniques that permit atomic scale characterization [1–5]. Using simplified model catalysts such as single crystals, various surface properties including atomic and electronic structure, composition, oxidation state, etc., could be identified by low-energy electron diffraction (LEED), X-ray and UV-photoelectron spectroscopy (XPS, UPS), Auger electron spectroscopy (AES), high-resolution electron energy loss spectroscopy (HREELS) and others [6,7]. Reactive molecules could be adsorbed on these surfaces and their structure, bonding and reactions could be studied with the available techniques. To better mimic technical catalysts, model systems of higher complexity were subsequently developed ranging from single crystal surfaces modified by oxide overlayers to vacuum-grown supported nanoparticles [8–12]. The major drawback of most commonly used surface-sensitive techniques (employing the scattering, absorption or emission of electrons, atoms and ions) is their need for ultrahigh vacuum (UHV) or low pressure ($<10^{-4}$ mbar, 1 mbar = 100 Pa), which prevents the use under reaction conditions.

Consequently, high-pressure studies of catalytic processes on single crystal or UHV-grown model catalysts were frequently carried out using UHV-compatible reactor cells that are enclosed in or attached to a UHV surface analysis chamber [13–18]. Utilizing this approach, the model catalyst is characterized before the reaction in UHV by surface-sensitive techniques, subsequently transferred into the reaction cell for high-pressure catalysis (at about 1 bar), and finally analyzed in UHV after the reaction.

However, in recent years it became apparent that it is important to study catalytically active surfaces under reaction conditions and not just before and after the reaction [19]. There is compelling evidence from studies over the past decade that adsorbates may restructure the catalyst surface and that this effect may be even more pronounced at the high pressures and temperatures employed in most chemical reactions. Consequently, adsorbed species present during a high-pressure reaction may be different from those observed in a pre- or post-reaction analysis of surfaces in vacuum or at low pressure [20,21]. Even if the catalyst surface structure remains unchanged upon gas exposure, important intermediates of high-pressure catalytic reactions may not be present under low-pressure conditions. If active species are weakly bound they may only appear at high pressure after all the strongly adsorbing sites on the surface are occupied by the stronger bonded species [22]. In this way, dominant species of low pressure studies may turn out to be mere spectators in the high-pressure reaction. Several surface-sensitive techniques have been developed that allow molecular level studies of surfaces under high pressure [19,21], among them IR-vis sum frequency generation (SFG) surface vibrational spectroscopy. SFG can operate in a pressure range from UHV to ambient conditions and is able to bridge the gap to traditional surface science experiments.

In an effort to combine the concepts mentioned above, we have designed an apparatus that allows to prepare and characterize model catalysts under well-controlled condi-

* To whom correspondence should be addressed.

1022-5528/01/0100-0019$18.00/0

tions in UHV, and to monitor adsorbates at elevated pressure or during a catalytic reaction by *in situ* SFG vibrational spectroscopy. The reaction rate and selectivity can be simultaneously measured by gas chromatography. To determine the performance of our apparatus we have revisited two prominent adsorption systems, i.e., CO adsorbed on Ni(100) and Pt(111), combinations of the most widely used probe molecule with highly reactive metals. Nickel is a selective catalyst for the methanation reaction while platinum is used, e.g., for CO and ammonia oxidation, reforming, etc. The results obtained at low pressure are compared to infrared reflection absorption spectroscopy (IRAS) and high-resolution electron energy loss spectroscopy (HREELS) data. High-pressure spectra were acquired up to 200 mbar and demonstrate the capability of our system to study catalytic reactions at realistic conditions.

2. IR-vis sum frequency generation vibrational spectroscopy

Infrared–visible sum frequency generation is a surface-specific vibrational spectroscopy that can operate from submonolayer coverages to atmospheric pressure. Its application to catalysis research was pioneered by Somorjai and coworkers. In this section we focus on those aspects of SFG spectroscopy that are specifically important for its use in catalysis, since the SFG process itself has been reviewed in detail in the literature [23–27].

To acquire an SFG vibrational spectrum of adsorbate molecules on a metal catalyst surface, two picosecond-laserpulses are spatially and temporally overlapped on the sample (figure 1). One input beam is in the visible range at fixed frequency (ω_{vis}), while the second one is tunable in the infrared (ω_{IR}) to probe the vibrational modes of the surface species. In a simplified picture, when the IR beam is tuned through a vibrational resonance of the adsorbate, it induces a vibrational transition from the ground state to an excited state and simultaneously the visible beam induces a transition to a higher energy virtual state through a Raman process. The high-energy virtual state relaxes by emitting a photon with a frequency being the sum of the two input photon frequencies ($\omega_{\mathrm{SFG}} = \omega_{\mathrm{IR}} + \omega_{\mathrm{vis}}$), resulting in the generation of an output beam in the visible region. By tuning the IR beam and monitoring the intensity of the SFG output, an adsorbate vibrational spectrum is obtained by plotting the SFG intensity vs. the IR wavenumber.

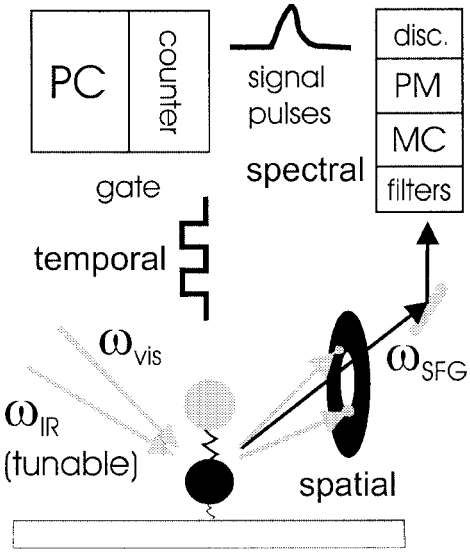

Figure 1. Schematic representation of the sum frequency generation process and the detection of the SFG-signal utilizing spatial, spectral and temporal filtering (MC – monochromator, PM – photomultiplier, disc. – discriminator).

The inherent surface-specificity of SFG originates from its second-order nonlinearity. As the IR beam is tuned through vibrational resonances of surface species, the surface nonlinear susceptibility $\chi_{\mathrm{s}}^{(2)}$ reaches a maximum. The intensity of the SFG signal is proportional to the absolute square of $\chi_{\mathrm{s}}^{(2)}$ and to the product of the incident light intensities. Beside the resonant term ($\chi_{\mathrm{R}}^{(2)}$), the surface itself may also contribute to the signal giving rise to a nonresonant background (however, $\chi_{\mathrm{NR}}^{(2)}$ is often invariant) [28]. Consequently,

$$I_{\mathrm{SFG}} \propto \left|\chi_{\mathrm{s}}^{(2)}\right|^2, \tag{1}$$

$$\chi_{\mathrm{s}}^{(2)} = \chi_{\mathrm{R}}^{(2)} + \chi_{\mathrm{NR}}^{(2)}, \tag{2}$$

$$\chi_{\mathrm{R}}^{(2)} = \sum_q \frac{A_q}{\omega_{\mathrm{IR}} - \omega_q + \mathrm{i}\Gamma_q}, \tag{3}$$

where $\chi_{\mathrm{R}}^{(2)}$, $\chi_{\mathrm{NR}}^{(2)}$, A_q, ω_q, ω_{IR} and Γ_q refer to the resonant nonlinear susceptibility, nonresonant nonlinear susceptibility, amplitude and resonant frequency of the qth vibrational mode, infrared laser frequency, and the damping constant of the qth vibrational mode (homogeneous linewidth $2\Gamma_q = \mathrm{FWHM}$), respectively. We can further write

$$A_q = \frac{1}{2\omega_q} \frac{\partial \mu_n}{\partial q} \frac{\partial \alpha_{lm}^{(1)}}{\partial q}, \tag{4}$$

where μ_n is the dipole moment, $\alpha_{lm}^{(1)}$ is the linear polarizability tensor, and accordingly $\partial\mu_n/\partial q$ and $\partial\alpha_{lm}^{(1)}/\partial q$ are the infrared dipole derivative and the Raman polarizability change for the normal mode q. Equation (4) clearly illustrates the selection rule for the SFG process. In order for a vibrational mode to be SFG active, it must simultaneously satisfy both infrared and Raman selection rules (in the electric dipole approximation). Therefore, SFG is not allowed in media with inversion symmetry since the mutual exclusive law prohibits a mode to be both IR and Raman active. Consequently, the lack of inversion symmetry is a prerequisite for SFG and, in the case of adsorption on face-centered cubic metals, the process can only occur at the surface where the inversion symmetry is broken. The dominant contribution to the SFG signal is hence generated by the modes of the adsorbed monolayer, while the centrosymmetric bulk of fcc metals and an isotropic gas phase give nearly-zero contribution to the signal. SFG can be carried out using different po-

larization combinations to gain information about molecular orientations, but all experiments reported here were made in (p,p,p) geometry, i.e., all beams were p-polarized [21].

Most SFG studies were performed on single crystals because very rough surfaces or microporous materials may scatter the beams and produce higher noise that would make the detection difficult. However, results on Pt foil were published [29] and we have recently obtained SFG spectra of CO adsorbed on Pd nanoparticles (4 nm in size) grown on well-ordered thin alumina films [30].

3. Experimental

The experiments were carried out in a two-level system that combines a UHV surface analysis chamber (base pressure 1×10^{-10} mbar, upper level) with an elevated pressure reactor (lower level) that is SFG- and UHV-compatible. With the help of an $xyz\varphi$ manipulator with 400 mm z-travel, the sample can be transferred between the two levels while maintaining a UHV environment.

A sample holder (or "cold finger", figure 2), which is basically a closed-end double-walled tube, is connected to the manipulator. A circular plate with four electrical feedthroughs (two Mo rods and a chromel–alumel thermocouple) is welded to the inside of the tube. The sample crystal is spotwelded to the Mo rods for resistive heating, and for temperature readings, a thin type K thermocouple is spotwelded to the rear of the crystal. After filling the inner tube with liquid N_2, a sample temperature of 85 K can be reached within 5 min. To avoid extensive cooling of the outside wall of the sample holder, the space in between the two tubes is evacuated. By resistive heating a temperature of 1300 K can be reached quickly.

The Ni(100) single crystal surface was cleaned in the UHV chamber (upper level) by Ar ion bombardment (beam energy 1 kV at 2×10^{-4} mbar Ar) while heated to 850 K within 2 h and annealed at 850 K for 2 min. Pt(111) was prepared in a similar manner, i.e., sputtered at 1 kV at 300 K for 20 min and subsequently annealed at 1250 K for 3 min. The surface structure and cleanliness of the sample surfaces were examined by low-energy electron diffraction (LEED), Auger electron spectroscopy (AES) and temperature-programmed desorption (TPD).

For vibrational studies and kinetic measurements, the specimen is transferred *in vacuo* into the SFG-compatible reaction cell (figure 2). When the manipulator is lowered to the SFG level, the sample holder is inserted into an arrangement of three differentially pumped spring-loaded teflon seals. The outside of the sample holder is mirror polished to provide a better sealing surface. The reaction cell can be pressurized to 1 bar while the upper chamber can still be kept at 5×10^{-10} mbar. Figure 2 shows a cross-section of the lower level of our chamber with the sample holder inserted, the flange housing the teflon seals, and the reaction cell. The reactor is equipped with two CaF_2 windows to allow infrared and visible light to enter, and to allow sum frequency light

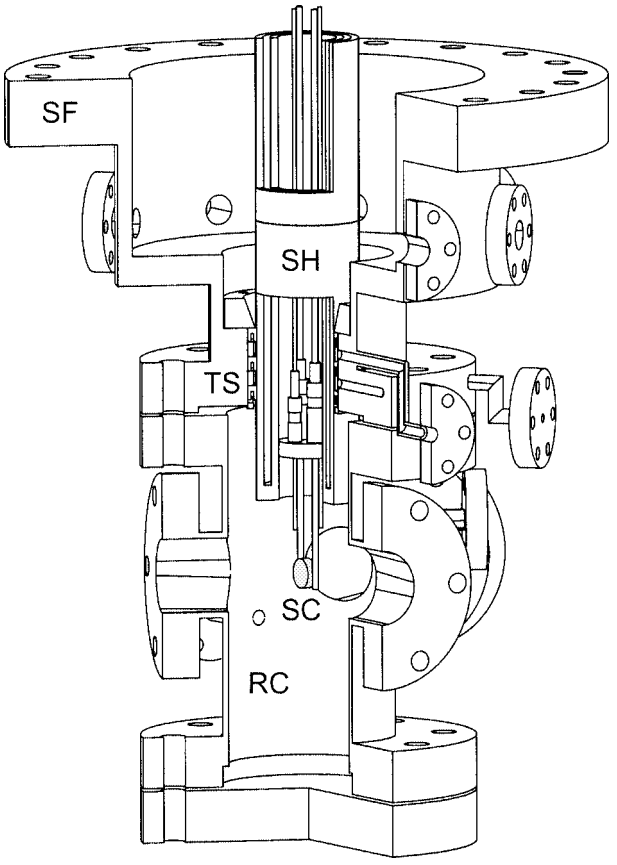

Figure 2. Cross-section showing the sample holder (SH), the sealing flange (SF) housing the differentially-pumped spring-loaded teflon seals (TS) and the reaction cell (RC). A single crystal (SC) is spotwelded to the sample holder that is inserted into the teflon seals. To minimize background activity, the walls of the reaction cell are gold coated.

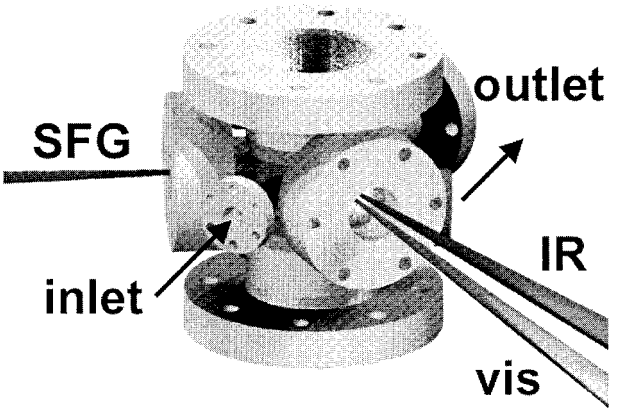

Figure 3. Alignment of the laser beams with respect to the SFG-reaction cell (reflected beams are not shown; see text).

to exit to the detector. The infrared and visible beams make an angle of about 55° and 50° with respect to the surface normal, respectively, and overlap at the sample surface. The difference in the incident angles of the beams is necessary to spatially separate the SFG signal from the reflected pump beams (figure 1). Figure 3 illustrates the orientation of the beams with respect to the reactor (reflected beams are not shown).

The source of the visible radiation (790 nm, 2 mJ/pulse, 2 ps, 500 Hz) is an amplified titanium sapphire laser, and 90% of the output is used to generate tunable infrared light (3–6 μm, ca. 10 μJ/pulse) with an optical parametric generator/amplifier (OPG/OPA). The infrared power is nearly constant between 2000 and 3300 cm^{-1}, but decreases below 2000 cm^{-1} due to a reduction of the transmission of the $AgGaS_2$ crystal in the OPG/OPA. The flange between the CaF_2 windows is used as a gas inlet so that when catalytic reactions are carried out, the gas mixture is directed onto the catalyst surface (figure 3). Two flanges on the back of the reactor are used as gas outlet and, in batch mode, they are connected to a metal bellows recirculation pump. The recirculation loop is interfaced with a gas chromatograph through an electric gas sampling valve. CO is introduced via a manifold after passing a cold trap (to remove carbonyl impurities) and the gas pressure is measured using a Baratron gauge. To apply low exposures in UHV experiments, a leak valve and an ionization gauge are connected to a flange on the back of the reactor.

Since the generation of an SFG signal is a very inefficient process, even with our high-power laser system (producing a surface power density on the order of 1 GW/cm^2), the absolute signal intensity is low. For instance, in the case of CO on Pt(111) 10^{14}–10^{15} photons per pulse of incident light produce only a few counts in the detector (detector sensitivity ~0.1%). However, the small signal can be detected by a combination of spatial, spectral and temporal filtering, as illustrated in figure 1. It has been mentioned that SFG is independent of gas pressure, but the absorption of infrared light at high pressure has still to be kept in mind. The intensity of the SFG signal critically depends on the intensity of the IR pulse arriving at the sample surface, which in turn, is influenced by gas phase absorption. Figure 4 shows SFG spectra of a GaAs reference crystal in 10^{-7}, 50, 100 and 200 mbar CO. The zincblende structure of GaAs exhibits no inversion symmetry, so GaAs produces a constant bulk SFG signal in 10^{-7} mbar CO (figure 4). The intensity variation at 50, 100 and 200 mbar CO is only due to the absorption of the IR beam in the gas phase. Similar plots were acquired for a number of gas pressures and used to normalize our SFG spectra, i.e., all high-pressure SFG spectra were corrected for gas phase absorption. The IR frequency was calibrated to an accuracy of ± 3 cm^{-1} by measurements of the atmospheric CO_2 absorption bands around 2350 cm^{-1}. To prevent the attenuation of the IR beam by atmospheric CO_2 and water before entering the chamber, all beam lines are encapsulated and purged with dry nitrogen.

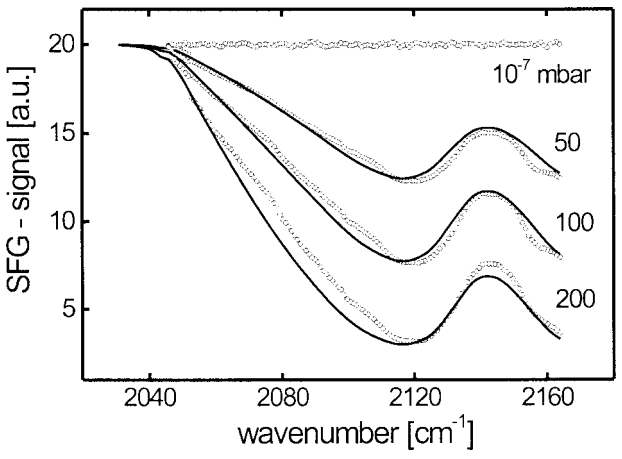

Figure 4. Effect of CO gas phase absorption on the SFG-signal from a GaAs reference crystal. The experimental data points (○) were fitted using the Lambert–Beer equation (—).

4. Results

4.1. Adsorption of CO on Ni(100) at low pressure

Nickel is an important catalytic material, e.g., for selective methanation, and the adsorption of CO and the promotion of C–O bond hydrogenation on supported Ni by the oxide–metal interface have attracted much attention [2,31]. However, some aspects are still under debate (for a review see [32]). CO on Ni(100) exhibits a temperature-dependent site occupation and at coverages $\leqslant$0.5 monolayers (ML) there is no agreement on the ratio between on-top and bridge-bonded CO [33,34]. Ibach et al. [34] showed that the variation of the adsorption site occupancy at a fixed temperature also strongly depends on the total CO coverage. At coverages >0.5 a compressed overlayer is formed but two different structures were suggested: (i) an incommensurate overlayer of CO on Ni(100) [35], and (ii) a coincidence structure [36]. To allow a comparison of our SFG spectra with IRAS and HREELS data, low pressures were applied.

As mentioned in section 3, the Ni(100) single crystal surface was cleaned by repeated sputter/anneal cycles and the cleanliness was checked by AES. Carbon was found to be the most resistant impurity (originating from bulk C segregation). It occupies fourfold hollow sites on the surface and forms a very stable c(2×2) structure on Ni(100) as observed by LEED (figure 5; or more precisely a p4g, see [7,37]). Remaining traces of surface carbon were removed by oxidation in 1×10^{-6} mbar O_2 at 570 K (5 min). After this treatment, oxygen was found on the surface by AES but could be removed by 1×10^{-6} mbar H_2 at 750 K (30 min) and a clean (1×1) surface was obtained.

A series of CO-TPD spectra of Ni(100) is shown in figure 6, together with the corresponding uptake curve obtained by integration of the peak areas. Upon adsorption of 0.5 L CO (1 L = 1 langmuir = 10^{-6} Torr s) at 100 K, high binding energy adsorption sites at 420 K are occupied predominantly. Using the Redhead formula, the adsorption energy was estimated to be 110 kJ/mol. Higher CO exposures reduce the desorption temperature of this species up to 10 K due to repulsive interactions between CO molecules that decrease the heat of adsorption. Exposures >1 L (>0.25 ML) produce additional desorption peaks around 350 and 280 K. At coverages $\leqslant$0.5 ML (~2 L), CO forms an ordered c(2×2) structure [35] but at higher coverages a compressed overlayer is formed. This makes the desorption process rather

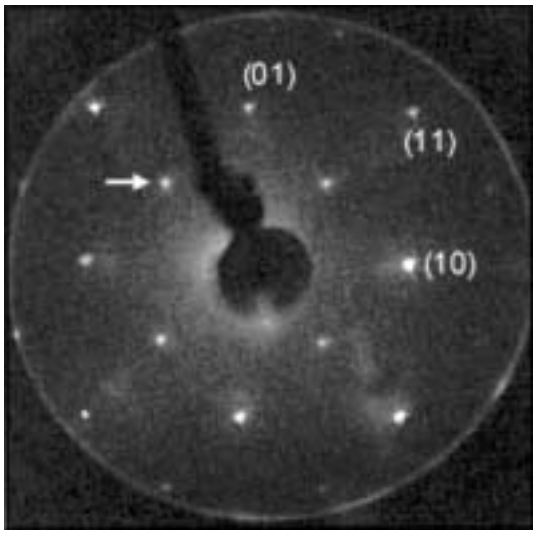

Figure 5. LEED pattern of Ni(100) c(2×2)C at 100 K (125 eV). One carbon spot is marked by an arrow.

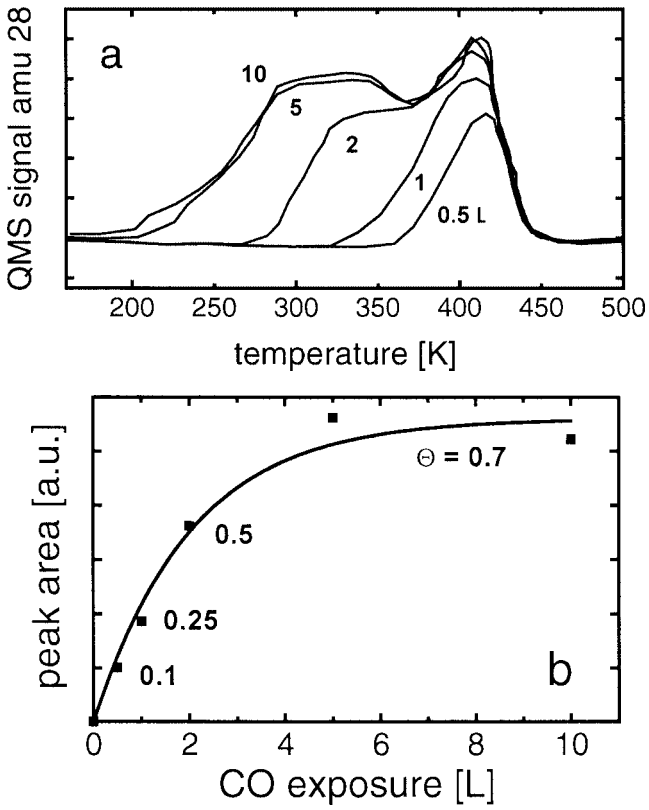

Figure 6. (a) TPD spectra for different CO exposures on Ni(100) at 100 K collected at a heating rate of 2 K/s (exposure indicated in langmuirs). (b) CO uptake curve calculated from the TPD spectra shown in (a); the saturation coverage at 300 K when CO forms an ordered c(2 × 2) structure with $\Theta = 0.5$ was used as reference [33].

complicated [38], which is reflected by the emergence of the low-temperature peaks at high coverages. The 420 K desorption peak was found to be at least equally sensitive to surface carbon as Auger spectroscopy. Carbon in four-fold hollow sites seems to hinder the adsorption of CO on the high binding energy sites while the broad peaks at 280 and 350 K were less affected. When the 420 K peak was absent, i.e., when carbon was present, no adsorbates could be detected by SFG. It seems likely that small amounts of carbon impurities may account for the different adsorption geometries reported in the literature. It has also been suggested that carbon species on Ni surfaces may act as precursor in the methanation reaction [2,31].

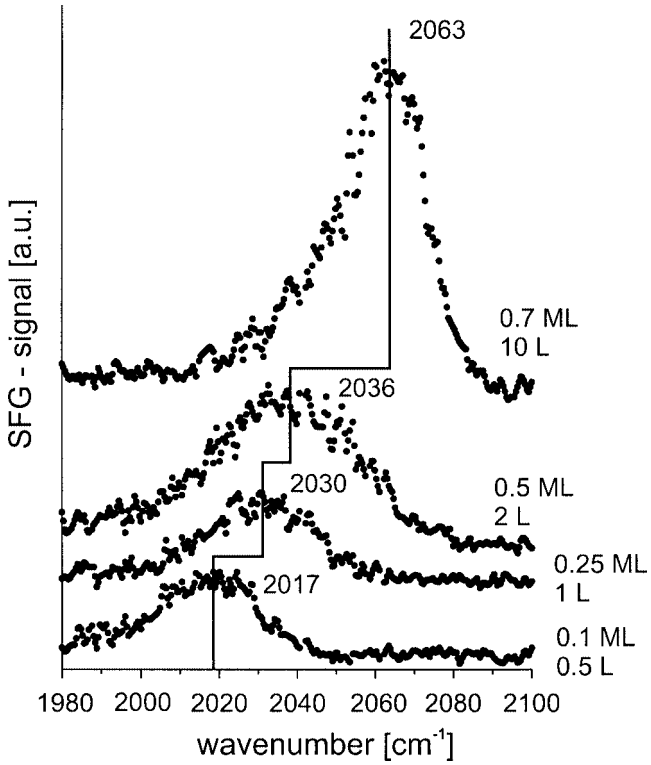

Figure 7. SFG spectra of CO adsorption on Ni(100) at 100 K for different exposures. The observed resonance feature is characteristic of terminally bonded (on-top) CO.

Figure 7 shows the SFG spectra of CO adsorption on Ni(100) at 100 K for different exposures. The nonlinear SFG response from the clean Ni(100) surface was constant between 1950 and 2200 cm^{-1}. We could not detect bridge-bonded CO but the small IR intensity of our setup below 2000 cm^{-1} could account for the absence of bridge-bonded CO in the spectra. Therefore, we will focus on the on-top species. After exposing Ni(100) at 100 K to 0.5 L CO (i.e., ∼0.1 ML) a single resonance feature characteristic of the stretching vibration of terminally bonded (on-top) CO was observed. The desorption peak at 420 K is therefore attributed to on-top CO, while the lower temperature peaks are rather connected to the compressed overlayer. This is supported by the consideration that carbon in four-fold hollow sites strongly interferes with atop Ni sites and hence prevents linear bonding. With increasing CO coverage the frequency of the CO peak shifted from 2017 cm^{-1} at 0.5 L (∼0.1 ML), to 2030 cm^{-1} at 1 L (∼0.25 ML), to 2036 cm^{-1} at 2 L (∼0.5 ML; c(2 × 2)) and to 2063 cm^{-1} at 10 L (∼0.7 ML). As the packing density of CO increases, there

is an enhancement in the dipole coupling between the CO molecules on the surface and a weakening of their bonds to the metal (cf. figure 6), resulting in the observed frequency shift. This shift is in good agreement with IRAS, HREELS and SFG studies carried out below half monolayer coverage [27,33,39–41].

At coverages >0.5, the IRA and EEL spectra in [33,39, 42] exhibit a broad band between 2000 and 2100 cm^{-1}, indicating that a distinct terminal site no longer exists. Therefore, it has been suggested that CO molecules are arranged in incommensurate adsorbate layers. The SFG spectra that we acquired at saturation coverage of CO (e.g., 10 L or more) did not show a broad band but still exhibited a single peak at 2063 cm^{-1}. A similar result was obtained in an EELS study by Uvdal et al. [40] who observed both on-top and bridge sites at $\Theta = 0.6$ and in an FT-IRAS study by Ibach [34]. The presence of a distinct on-top CO peak at $\Theta > 0.5$ supports the coincidence structure models suggested by Biberian and van Hove [36] for the compressed overlayer, since these models allow one to place CO molecules in well-specified (high symmetry) on-top and bridge sites. High-pressure studies on Ni are complex due to the fast dissociation of CO, rapid carbon build-up and the formation of volatile Ni carbonyls at higher temperatures. Studies of CO adsorption at high pressures were therefore carried out on Pt(111).

4.2. Adsorption of CO on Pt(111) from 10^{-7} to 200 mbar

To expose a clean metal surface to high gas pressures may have different effects. As recently observed by scanning tunneling microscopy (STM), near-atmospheric pressures of CO, H_2 or O_2 may alter a Pt(110) [43] and Pt(111) [44] surface (adsorbate-induced restructuring). Such structural changes should also show up in SFG spectra of adsorbed molecules and Somorjai et al. [45] reported the formation of Pt–carbonyl species on Pt(111) at 300 K at CO pressures higher than 15 mbar. The carbonyls were coadsorbed with an incommensurate CO overlayer. When a Rh(111) surface was exposed to 900 mbar CO, a CO species bound to defect sites was detected by SFG, besides on-top CO [21]. STM-studies of Rh(111) [46] and of UHV-grown Rh nanoparticles supported on oxide single crystals report similar effects after extended gas exposure ("particle disrupture") [47]. Even if a high gas pressure does not restructure a metal surface, it is very likely that the ratio between different adsorbed species (e.g., on-top vs. bridge) may significantly depend on gas pressure. The adsorption of CO on Pt(111) has already received much attention, but most molecular studies were carried out at very low pressures. Therefore, it seems worthwhile to re-examine this system and to extend the pressure to near atmospheric conditions.

As mentioned in section 3, SFG makes use of high-power laser pulses and each of our spectra takes about 10–20 min. To rule out the possibility of laser-induced photodesorption or thermal desorption of CO, we have carried out a series of TPD experiments. The Pt(111) surface was exposed to, e.g., 2 L CO at 230 K and a TPD spectrum was acquired (figure 8). Thereafter, the surface was again exposed to 2 L CO and subsequently transferred to the high-pressure cell. After an SFG spectrum was taken, the Pt crystal was transferred back in the surface analysis chamber and another TPD spectrum was taken. As demonstrated by figure 8, we could not detect any change in surface coverage resulting from sample transfer or spectroscopy.

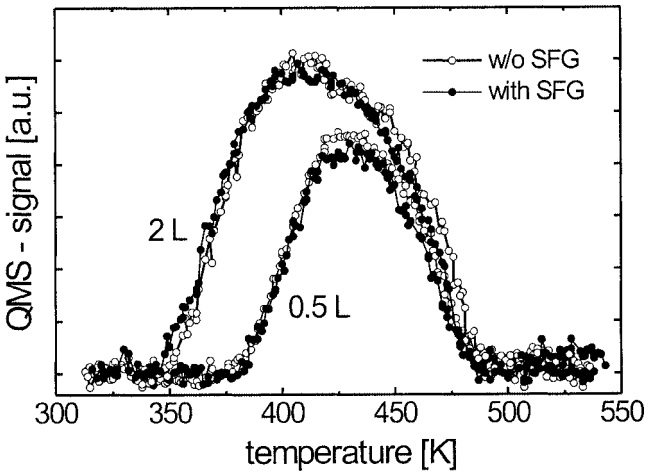

Figure 8. TPD spectra for different CO exposures on Pt(111), taken directly after dosing (○) and after sample transfer and subsequent acquisition of an SFG spectrum (●); see text (heating rate 2 K/s; exposure indicated in langmuirs). The agreement of the TPD traces indicates the absence of significant laser-induced desorption.

Figure 9 displays SFG spectra of CO adsorption on Pt(111) at 230 K from 10^{-7} to 200 mbar. The nonlinear response from the clean Pt surface was small but constant over the spectral region shown. At 10^{-7} mbar CO, a single resonance feature at 2097 cm^{-1} was observed which is characteristic of the C–O stretching vibration of terminally adsorbed CO. In agreement with earlier studies, at saturation coverage (∼2 L) a c(4 × 2) LEED pattern was observed [48,49], corresponding to a superstructure in which an equal number of CO molecules occupy on-top and bridge sites ($\Theta \approx 0.5$). While the resonance frequency of on-top CO agrees well with previous HREELS [50], IRAS [51,52] and SFG [45,53,54] studies, the absence of bridge-bonded CO (expected around 1850 cm^{-1}) in our spectra is again probably due to our low IR energy below 1900 cm^{-1}.

The SFG spectra taken at higher CO pressure were corrected for gas phase absorption, as mentioned in section 3. It should be noted that a LN_2 trap was used to purify CO because at these pressures even impurities in the range of 10^{-3}% have a considerable partial pressure. Increasing the CO pressure up to 200 mbar did not shift the frequency and on-top CO was the only species detected in our experiments. This indicates that the adsorption geometry of CO on Pt(111) at 230 K is independent of gas pressure. High-pressure SFG studies at higher temperatures are in progress.

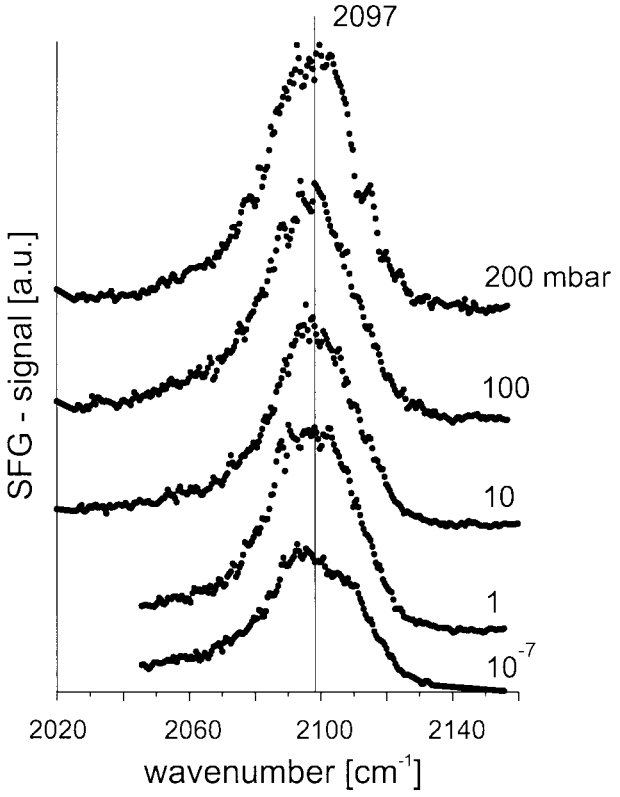

Figure 9. SFG spectra of CO adsorption on Pt(111) at 230 K in the pressure range from 10^{-7} to 200 mbar. The spectra above 10^{-7} mbar were corrected for CO gas phase absorption. Terminally bonded (on-top) CO is the only species detected.

5. Conclusions and future perspectives

We have set up an instrument that enables us to prepare and characterize well-defined model catalysts in UHV, and to transfer them *in vacuo* into an SFG-compatible elevated pressure reactor. Studies of CO adsorption on Ni(100) indicate that CO adsorbs on on-top sites at coverages $\leqslant$0.5 ML, and favor the coincidence structure models for higher coverages. On Pt(111), the adsorption of CO at 230 K was monitored in the range from 10^{-7} to 200 mbar. CO was found to adsorb on on-top sites independent of gas pressure.

At present, we are setting up a new OPG/OPA system to improve our resolution and to increase the IR-energy below 2000 cm^{-1}. SFG can also be applied to study oxide surfaces. In preliminary studies of CO and NO adsorption on epitaxially grown NiO(100), the C–O stretching frequency was found close to the C–O gas phase value, as a result of the weak interaction with the oxidic substrate, while the N–O stretching frequency was shifted to lower wavenumbers ($\sim$1780 cm^{-1}) due to the chemical bonding to the surface. SFG-studies of catalytic reactions at high gas pressure will be started in the near future.

Since very rough surfaces or microporous materials scatter the beams and produce high noise, SFG studies are often carried out on single crystals. However, we have recently succeeded in acquiring SFG spectra from 3 nm Pd particles grown on well-ordered thin alumina films [30]. The application of SFG spectroscopy to supported metals should significantly contribute to our understanding of catalytic processes.

Currently, the intensity of SFG spectra is generally given in arbitrary units. This rather unsatisfactory situation originates from problems to put SFG on a quantitative basis. The intensity of the SFG signal depends on the laser performance, the optical alignment, detector sensitivity, etc. Therefore, our spectra are referenced to the bulk SFG signal of a GaAs crystal and all spectra collected in a figure are measured on the same day. Ideally, the visible and IR beams should be split and a GaAs reference spectrum should be acquired simultaneously with every SFG spectrum. In this way small variations in laser power could be corrected. In addition, the reference cell should contain the same gas composition as the reaction cell to account for gas phase absorption. The small IR energy of our current setup prevents the implementation of such a reference cell, but will be possible with our new system.

At present, SFG spectroscopy in scanning mode is slow, but improvements are possible by using broadband techniques [55]. A broad-bandwidth IR pulse is mixed with a narrow-bandwidth visible pulse and the resulting SFG spectrum is dispersed with a spectrograph and detected with a CCD-camera. Using this technique, fast and high S/N ratio data acquisition over a spectral range of 400 cm^{-1} is possible without scanning the IR frequency. Moreover, time resolved SFG, in the form of pump–probe experiments, is able to examine dynamic surface processes [56]. SFG spectroscopy is currently limited to wavenumbers above 1000 cm^{-1} but the development of new and better nonlinear crystals could resolve that problem. The utilization of a free-electron laser extends the frequency range to the far-infrared and allows to study metal–adsorbate vibrational modes [57]. The high pressure capability of SFG, combined with improved frequency- and time-resolution, will make sum frequency generation spectroscopy an indispensable *in situ* diagnostic tool to study catalytic processes on a molecular level.

References

[1] J.M. Thomas and W.J. Thomas, *Principles and Practice of Heterogeneous Catalysis* (VCH, Weinheim, 1997).
[2] G.A. Somorjai, *Introduction to Surface Chemistry and Catalysis* (Wiley, New York, 1994).
[3] G.A. Somorjai, Chem. Rev. 96 (1996) 1223.
[4] D.W. Goodman, Chem. Rev. 95 (1995) 523.
[5] G. Ertl, Surf. Sci. 299/300 (1994) 742.
[6] D.P. Woodruff and T.A. Delchar, *Modern Techniques of Surface Science* (Cambridge Univ. Press, New York, 1986).
[7] G.A. Somorjai and G. Rupprechter, J. Chem. Educ. 75 (1998) 161.
[8] H.-J. Freund, Angew. Chem. Int. Ed. Engl. 36 (1997) 452.
[9] C.R. Henry, Surf. Sci. Rep. 31 (1998) 235.
[10] G. Rupprechter, K. Hayek and H. Hofmeister, J. Catal. 173 (1998) 409.
[11] A. Eppler, G. Rupprechter, L. Guczi and G.A. Somorjai, J. Phys. Chem. B 101 (1997) 9973.
[12] M. Bäumer and H.-J. Freund, Prog. Surf. Sci. 61 (1999) 127.
[13] D.W. Blakely, E. Kozak, B.A. Sexton and G.A. Somorjai, J. Vac. Sci. Technol. 13 (1976) 1091.
[14] G. Rupprechter and G.A. Somorjai, Catal. Lett. 48 (1997) 17.

[15] S.M. Davis, F. Zaera and G.A. Somorjai, J. Am. Chem. Soc. 104 (1982) 7453.
[16] D.W. Goodman, R.D. Kelley, T.E. Madey and J.T. Yates, J. Catal. 63 (1980) 226.
[17] R.A. Campbell and D.W. Goodman, Rev. Sci. Instrum. 63 (1992) 172.
[18] C. Sellmer, A. Gaussmann, N. Kruse and R. Prins, J. Vac. Sci. Technol. A 15 (1997) 365.
[19] J.M. Thomas and G.A. Somorjai, eds., Topics Catal. 8 (1999), special issue on *In Situ Characterization of Catalysts*.
[20] X. Su, J. Jensen, M.X. Yang, M.B. Salmeron, Y.R. Shen and G.A. Somorjai, Faraday Discuss. 105 (1996) 263.
[21] G.A. Somorjai and G. Rupprechter, J. Phys. Chem. B 103 (1999) 1623.
[22] P.S. Cremer, X. Su, Y.R. Shen and G.A. Somorjai, J. Am. Chem. Soc. 118 (1996) 2942.
[23] Y.R. Shen, Nature 337 (1989) 519.
[24] Y.R. Shen, Surf. Sci. 299/300 (1994) 551.
[25] Y.R. Shen, *The Principles of Nonlinear Optics* (Wiley, New York, 1984).
[26] X.D. Zhu, H. Suhr and Y.R. Shen, Phys. Rev. B 35 (1987) 3047.
[27] J. Miragliotta, P. Rabinowitz, S.D. Cameron and R.B. Hall, Appl. Phys. A 51 (1990) 221.
[28] J.H. Hunt, P. Guyot-Sionnest and Y.R. Shen, Chem. Phys. Lett. 133 (1987) 189.
[29] H. Härle, A. Lehnert, U. Metka, H.R. Volpp, L. Willms and J. Wolfrum, Chem. Phys. Lett. 293 (1998) 26.
[30] T. Dellwig, G. Rupprechter, H. Unterhalt and H.-J. Freund, Phys. Rev. Lett. 85 (2000) 776.
[31] D. Kelley and D.W. Goodman, Chem. Phys. Sol. Surf. Het. Catal. 4 (1982) 435.
[32] J.C. Campuzano, in: *The Chemical Physics of Solid Surfaces and Heterogeneous Catalysis*, Vol. 3, Part A, eds. D.A. King and D.P. Woodruff (Elsevier, Amsterdam, 1990) p. 389.
[33] J. Lauterbach, M. Wittmann and J. Küppers, Surf. Sci. 279 (1992) 287.
[34] A. Grossmann, W. Erley and H. Ibach, Surf. Sci. 330 (1995) L646.
[35] J.C. Tracy, J. Chem. Phys. 56 (1972) 2736.
[36] J.P. Biberian and M.A. van Hove, Surf. Sci. 118 (1982) 443.
[37] Y. Gauthier, R. Baudoing-Savois, K. Heinz and H. Landskron, Surf. Sci. 251 (1991) 493.
[38] S. Johnson and R.J. Madix, Surf. Sci. 108 (1981) 77.
[39] S. Andersson, Solid State Commun. 88 (1993) 1085.
[40] P. Uvdal, P.A. Karlsson, S. Andersson and N.V. Richardson, Surf. Sci. 202 (1988) 167.
[41] J. Yoshinobu and M. Kawai, Surf. Sci. 368 (1996) 239.
[42] R. Klauser, W. Spieß and A.M. Bradshaw, J. Electron Spectrosc. Relat. Phenom. 38 (1986) 187.
[43] B.J. McIntyre, M.B. Salmeron and G.A. Somorjai, Rev. Sci. Instrum. 64 (1993) 687.
[44] J.A. Jensen, K.B. Rider, M. Salmeron and G.A. Somorjai, Phys. Rev. Lett. 80 (1998) 1228.
[45] X. Su, P.S. Cremer, Y.R. Shen and G.A. Somorjai, Phys. Rev. Lett. 77 (1996) 3858.
[46] J. Jensen, K. Rider, Y. Chen, M. Salmeron and G. Somorjai, J. Vac. Sci. Technol. B 17 (1999) 1080.
[47] A. Berkó, G. Ménesi and F. Solymosi, J. Phys. Chem. 100 (1996) 17732.
[48] H. Steininger, S. Lehwald and H. Ibach, Surf. Sci. 117 (1982) 342.
[49] G. Ertl, M. Neumann and K.M. Streit, Surf. Sci. 64 (1977) 393.
[50] N.R. Avery, J. Chem. Phys. 74 (1981) 4202.
[51] C.W. Olsen and R.I. Masel, Surf. Sci. 201 (1988) 444.
[52] B.E. Hayden and A.M. Bradshaw, Surf. Sci. 125 (1983) 787.
[53] C. Klünker, M. Balden, S. Lehwald and W. Daum, Surf. Sci. 360 (1996) 104.
[54] H. Härle, K. Mendel, U. Metka, H.R. Volpp, L. Willms and J. Wolfrum, Chem. Phys. Lett. 279 (1997) 275.
[55] L.T. Richter, T.P. Petrallimallow and J.C. Stephenson, Opt. Lett. 23 (1998) 1594.
[56] H. Ueba, Prog. Surf. Sci. 55 (1997) 115.
[57] C.T. Williams, Y. Yang and C.D. Bain, Catal. Lett. 61 (1999) 7.